BIOCHEMISTRY

Nitrogen isotope signature evidences ammonium deprotonation as a common transport mechanism for the AMT-Mep-Rh protein superfamily

Idoia Ariz[1]*†, Mélanie Boeckstaens[2], Catarina Gouveia[1], Ana Paula Martins[3], Emanuel Sanz-Luque[4‡], Emilio Fernández[4], Graça Soveral[3], Nicolaus von Wirén[5], Anna M. Marini[2], Pedro M. Aparicio-Tejo[6], Cristina Cruz[1]*

Ammonium is an important nitrogen (N) source for living organisms, a key metabolite for pH control, and a potent cytotoxic compound. Ammonium is transported by the widespread AMT-Mep-Rh membrane proteins, and despite their significance in physiological processes, the nature of substrate translocation (NH_3/NH_4^+) by the distinct members of this family is still a matter of controversy. Using *Saccharomyces cerevisiae* cells expressing representative AMT-Mep-Rh ammonium carriers and taking advantage of the natural chemical-physical property of the N isotopic signature linked to NH_4^+/NH_3 conversion, this study shows that only cells expressing AMT-Mep-Rh proteins were depleted in ^{15}N relative to ^{14}N when compared to the external ammonium source. We observed ^{15}N depletion over a wide range of external pH, indicating its independence of NH_3 formation in solution. On the basis of inhibitor studies, ammonium transport by nonspecific cation channels did not show isotope fractionation but competition with K^+. We propose that kinetic N isotope fractionation is a common feature of AMT-Mep-Rh–type proteins, which favor ^{14}N over ^{15}N, owing to the dissociation of NH_4^+ into $NH_3 + H^+$ in the protein, leading to ^{15}N depletion in the cell and allowing NH_3 passage or NH_3/H^+ cotransport. This deprotonation mechanism explains these proteins' essential functions in environments under a low NH_4^+/K^+ ratio, allowing organisms to specifically scavenge NH_4^+. We show that ^{15}N isotope fractionation may be used in vivo not only to determine the molecular species being transported by ammonium transport proteins, but also to track ammonium toxicity and associated amino acids excretion.

INTRODUCTION

Ammonium (unless a distinction is made, the term ammonium used in this paper refers to both chemical forms: NH_4^+ and NH_3) is a major nitrogen (N) source for living organisms and supports tumor proliferation (*1*–*3*). It is not only a key metabolite in the control of systemic pH by the kidney but also a potent cytotoxic compound (*1*–*4*). The conversion of the ionic (NH_4^+) to the neutral (NH_3) form depends on pH and temperature, with a pK_a (where K_a is the acid dissociation constant) ≈ 9.25 at 25°C (pK_a ≈ 9.09 at 30°C); thus, at pH 7 and below, more than 99% of ammonium in solution is present in its ionic form. Ammonium transport across biological membranes was initially thought to occur mainly through NH_3 diffusion while it was later reconsidered to also proceed via carrier-mediated NH_4^+ transport (*5*–*7*). At low external substrate concentrations, ammonium transport across membranes occurs via AMT-Mep-Rh proteins, which are highly selective against K^+, despite the latter sharing a similar ionic radius with hydrated NH_4^+ ions (*6*–*8*). The AMT-Mep-Rh protein family is divided into two main subfamilies: ammonium transporters (AMT)–methylammonium/ammonium permeases (Meps) and rhesus (Rh) proteins. Most AMT-Mep proteins have been characterized as high-affinity ammonium transport systems, with K_m values generally in the micromolar range (*7*, *8*). Rh proteins are phylogenetically more distantly related and transport ammonium with lower affinity (K_m values in the millimolar range) (*1*, *9*, *10*). This highly conserved superfamily of membrane proteins is present in organisms belonging to all main lineages of life, including bacteria, fungi, algae, plants, and animals (*9*). Following the discovery and functional characterization of this protein family and the solving of the first three-dimensional (3D) structures, the question whether NH_3 or NH_4^+ is the transported substrate arose (*6*–*8*, *11*, *12*).

Heterologous expression of plant AMT transporters in *Xenopus laevis* oocytes and electrophysiological characterization using the two-electrode voltage clamp technique suggest an electrogenic transport mechanism for AMT1-type proteins (*9*, *13*). This mechanism may, for instance, correspond to the transport of NH_4^+ or the cotransport of H^+ and NH_3. In contrast, an electroneutral transport mechanism is proposed for AMT2-type transporters (*14*).

On the basis of the structures of AMT-Mep-Rh proteins, NH_3 is proposed to be the form transported for several members of the AMT-Mep-Rh protein family, typically characterized by a narrow hydrophobic pore between two hydrophilic regions, which constitute the periplasmic and cytoplasmic vestibules (*15*). The ionic form NH_4^+ appears to be the preferential form recruited in the periplasmic vestibule, and the constriction is proposed to allow NH_3, but not NH_4^+, to permeate the transporter (*11*, *15*). However, these static views are not sufficient to accurately determine the transport

[1]Centre for Ecology, Evolution and Environmental Changes, Faculdade de Ciências da Universidade de Lisboa, 1749-016 Lisboa, Portugal. [2]Biology of Membrane Transport, Department of Molecular Biology, Université Libre de Bruxelles, 6041 Gosselies, Belgium. [3]iMed.ULisboa–Research Institute for Medicines, Faculdade de Farmácia da Universidade de Lisboa, 1649-003 Lisboa, Portugal. [4]Department of Biochemistry and Molecular Biology, Univeristy of Córdoba, 14071 Cordoba, Spain. [5]Department of Physiology and Cell Biology, Leibniz Institute for Plant Genetics and Crop Plant Research, Seeland, 06466 OT Gatersleben, Germany. [6]Departamento de Ciencias, Universidad Pública de Navarra, 31006 Pamplona, Spain.
*Corresponding author. Email: iariza@unav.es (I.A.); ccruz@fc.ul.pt (C.C.)
†Present address: Departamento de Biología Ambiental, Facultad de Ciencias, Universidad de Navarra, Calle de Irunlarrea 1, Navarra, 31008 Pamplona, Spain.
‡Present address: Grossman Lab, Department of Plant Biology, Carnegie Institution for Science, 260 Panama Street, Stanford, CA 94305, USA.

mechanism. Overall, several possibilities for electrogenic or electroneutral ammonium transport exist. For electrogenic transport, NH_4^+ may be carried alone (uniport) or together with an H^+ (NH_4^+-H^+ symport). Alternatively, NH_4^+ may be recruited, deprotonated in the periplasmic vestibule, and carried as NH_3 together with an H^+ (NH_3-H^+ symport). In case of electroneutral transport, the possibilities include NH_3 uniport following direct recruitment of NH_3 from the external medium, NH_4^+ recruitment and deprotonation before NH_3 transport through the pore, or NH_4^+/H^+ antiport (fig. S1) (*9*).

In solution, NH_4^+ and NH_3 present distinct N isotopic compositions owing to differences in the equilibrium constants for the two isotopologues ^{15}N and ^{14}N (*16*). NH_4^+ ions containing ^{14}N are more easily deprotonated than those containing ^{15}N, leading to an isotopic fractionation linked to an isotope effect, α, at 30°C, of 1.044 between NH_4^+ and NH_3 (*17*). Thus, in equilibrium, NH_3 is depleted for ^{15}N by 44.3 milliUreys (mUr) relative to NH_4^+. Isotope fractionation occurs, in general, against the heavier isotope (for example, ^{15}N) and may originate from a kinetic or a thermodynamic isotope effect. The kinetic effect relates to the difference in reaction rate constants, and the thermodynamic one relates to the equilibrium constants (*16*). Therefore, cells transporting NH_3 or $NH_3 + H^+$ across their membranes will become ^{15}N-depleted compared to the external ammonium source as long as the ammonium source is not limited. To date, this isotopic fractionation against ^{15}N in the specific conversion of NH_4^+ into NH_3 has not yet been used to address AMT-Mep-Rh–mediated transport processes.

Here, we used ^{15}N isotope fractionation associated with pH-dependent NH_4^+ deprotonation, that is, equilibrium isotope effect of ammonium, to study the transport mechanisms of different ammonium-transporting proteins in living cells. This approach allowed us to assign NH_4^+ and NH_3 as substrates for different types of ammonium-transporting proteins in a noninvasive way. Furthermore, we studied the presence/absence of a kinetic isotope effect linked to the protein transport as a means to determine the N species transported (NH_4^+ or $NH_3 + H^+$) by ammonium membrane transport proteins. These studies support the acquisition and subsequent dissociation of NH_4^+ into NH_3 and H^+ by AMT-Mep-Rh–type proteins by a kinetic N isotope effect as a common transport mechanism of this protein superfamily.

RESULTS

Yeast ^{15}N depletion depends on the presence of *Sc*Mep proteins

We first investigated the influence of the three endogenous Mep ammonium transport proteins, *Sc*Mep1 to *Sc*Mep3, from *Saccharomyces cerevisiae* using Σ1278b as a wild-type strain grown under two different nutritional conditions. After 48 hours of growth, all tested yeast strains showed a similar optical density at 600 nm (OD_{600}) when grown at high ammonium concentrations (Fig. 1A). However, at low ammonium, triple-*mep*Δ cells were not able to grow (Fig. 1B). Consistent with previous reports, the presence of at least one of the three *Sc*Mep proteins was essential for yeast growth at low ammonium concentrations (*6*, *18*).

We next used isotope-ratio mass spectrometry (IRMS) to determine ^{15}N versus ^{14}N isotope discrimination during ammonium uptake. When grown at 76 mM ammonium for 48 hours (Fig. 1A), only *Sc*Mep-containing yeast cells, either wild type or the triple *mep*Δ

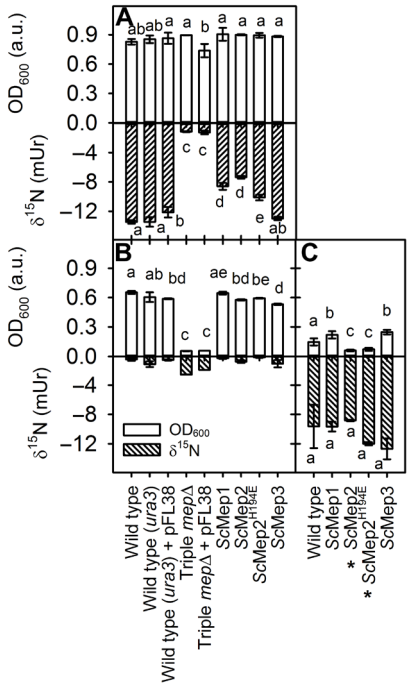

Fig. 1. Functional AMT-Mep–type proteins deplete cells in ^{15}N. Yeast growth (top) and natural N isotopic abundance (bottom) in yeast strains grown for 48 hours (**A** and **B**) or 20 hours (**C**) at pH 4.3 in the presence of 13 mM K^+ and 76 mM ammonium (A) or 1 mM ammonium (B and C). Wild type, Σ1278b; wild type (*ura3*), 23344c; wild type (*ura3*) + pFL38, wild type (*ura3*) + empty plasmid; triple *mep*Δ, 31019b; triple *mep*Δ + pFL38, triple *mep*Δ + empty plasmid; *Sc*Mep1, triple *mep*Δ + *Sc*Mep1; *Sc*Mep2, triple *mep*Δ + *Sc*Mep2; *Sc*Mep2^{H194E}, triple *mep*Δ + *Sc*Mep2^{H194E}; *Sc*Mep3, triple *mep*Δ + *Sc*Mep3 yeast strains. Data are presented as means ± SE ($n \geq 3$). Letters represent significant differences among yeast strains for a given ammonium concentration ($P \leq 0.05$). *Significant differences between ammonium concentrations for a given yeast strain. $\delta^{15}N$ of $(NH_4)_2SO_4$, 0.0 to 0.5 mUr. a.u., arbitrary units.

complemented with either *Sc*Mep1, *Sc*Mep2, or *Sc*Mep3, showed ^{15}N depletion relative to the N source; that is, the cellular $\delta^{15}N$ was more negative than the value for the N source; $\delta^{15}N$ of $(NH_4)_2SO_4 \approx$ 0 to 0.5 mUr. After growth at 1 mM ammonium for 48 hours, that is, $OD_{600} > 0.3$, pH 4.3 yeast cells did not show significant depletion of ^{15}N compared to their N source (Fig. 1B), as they consumed almost all the ammonium available in the culture medium (fig. S2). However, the cell ^{15}N depletion determined, at $OD_{600} < 0.3$, when N in the medium was not depleted (fig. S2) in relation to the N source (Fig. 1C), was similar to that observed for cells grown at 76 mM for 48 hours (Fig. 1A).

Cells expressing different types of ammonium-transporting proteins (that is, endogenous *Sc*Mep proteins; a tonoplast intrinsic protein, *Ta*TIP2;1, from *Triticum aestivum*, known to transport NH_3; and *At*AKT1, a K^+ permease from *Arabidopsis thaliana*, further capable of NH_4^+ transport) were used to evaluate the relationship between the mechanism of ammonium transport, the associated cell $\delta^{15}N$, and pH dependency across a 2.5 to 6.5 range (Fig. 2) (*19*, *20*). For the particular case of *Ta*TIP2;1, cells were grown with galactose as carbon source instead of glucose, as the corresponding gene is placed under the control of a Gal promoter. In addition, cells were grown at higher pH values (6.5 to 8.0) to achieve a better complementation of the triple-*mep*Δ cells' growth

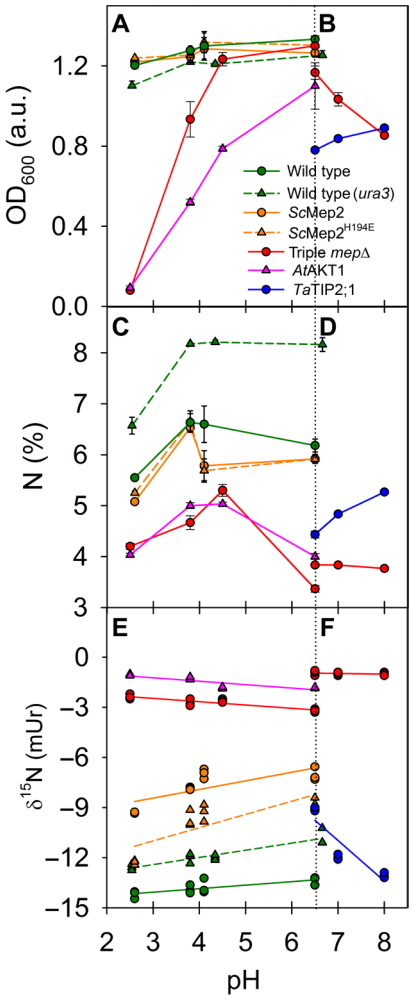

Fig. 2. Cellular $\delta^{15}N$ derived from Mep-, TIP-, and AKT-type transporters show differential pH dependence. Cell growth (OD_{600}; **A** and **B**), N content (%; **C** and **D**), and cellular N isotopic composition ($\delta^{15}N$; **E** and **F**). in Mep-containing cells and triple-*mep*Δ and yeast cells expressing other ammonium transporters. Yeast cells were grown at pH 4.3 in the presence of 13 mM K^+ and 76 mM ammonium. Yeast strains used in this study include wild-type (Σ1278b), triple *mep*Δ (31019b), wild-type (*ura3*) (23344c), triple *mep*Δ + *Sc*Mep2, and triple *mep*Δ + *Sc*Mep2^{H194E}. Other putative carriers of NH_4^+ (such as *At*AKT1 from *A. thaliana*, triple *mep*Δ + *At*AKT1) or NH_3 (such as *Ta*TIP2;1 from *T. aestivum*, triple *mep*Δ + *Ta*TIP2;1) that are not members of the AMT-Mep-Rh family were also tested and considered controls for different ammonium transport mechanisms. *Ta*TIP2;1 from *T. aestivum*–containing cells and triple-*mep*Δ cells were grown on galactose (3%) at pH above 6.5 (B and D). Equations for regression curves displayed in (A): wild type: $y = 0.21x - 14.69$, $R^2 = 0.5755$; wild type (*ura3*): $y = 0.43x - 13.70$, $R^2 = 0.8480$; triple *mep*Δ (on glucose; pH 2.5 to 6.5): $y = -0.2x - 1.87$, $R^2 = 0.7711$; triple *mep*Δ + *Sc*Mep2: $y = 0.52x - 9.98$, $R^2 = 0.5694$; triple *mep*Δ + *Sc*Mep2^{H194E}: $y = 0.79x - 13.38$, $R^2 = 0.6476$; triple *mep*Δ + *Ta*TIP2;1: $y = -2.42x + 5.99$, $R^2 = 0.8135$; triple *mep*Δ (on galactose; pH 6.5 to 8): $y = -0.04x - 0.70$, $R^2 = 0.0531$; triple *mep*Δ + *At*AKT1: $y = -0.21x - 0.61$, $R^2 = 0.7516$. $\delta^{15}N$ of $(NH_4)_2SO_4$, −1.0 to 0.5 mUr. Data are presented as means ± SE (A to D; $n = 3$).

defect by *Ta*TIP2;1 (*19*). At high external ammonium concentrations (76 mM), cell growth was strongly dependent on the presence of *Sc*Mep and pH (table S1). *Sc*Mep-expressing cells grew similarly in the range of pH from 2.5 to 6.5 (Fig. 2A). In contrast, the growth of triple-*mep*Δ cells, thus deprived of *Sc*Mep proteins, and of triple-*mep*Δ cells expressing *At*AKT1 or *Ta*TIP2;1 was dependent on pH (Fig. 2, A and B). Both *Sc*Mep presence and pH also influenced the cell N content (table S1). In general, cells lacking Mep proteins showed lower N content (Fig. 2, C and D), suggesting that at least a part of cell N supply may be provided by Mep proteins under high ammonium conditions. In addition, the cell $\delta^{15}N$ response to pH of the growth medium was differentially influenced by the pH range and the type of ammonium transport proteins (table S1 and Fig. 2, E and F). At pH below 6.5 (Fig. 2E), the strong dependence of cellular $\delta^{15}N$ on the presence of *Sc*Mep and its independence on pH, with no interaction of both factors (table S1), may indicate that the Mep-associated fractionation process is independent of the external pH and, therefore, of the concentration of NH_3 in the culture medium. However, triple-*mep*Δ cells, triple-*mep*Δ cells expressing *At*AKT1 (Fig. 2E), and triple-*mep*Δ cells expressing *Ta*TIP2;1 grown on galactose at pH from 6.5 to 8 (Fig. 2F) showed different pH responses. At pH below 6.5, in triple-*mep*Δ and triple-*mep*Δ *At*AKT1-expressing cells, pH had a contrasting effect on growth and on N content but had no effect on N isotope signature (Fig. 2). Neither of these strains, *mep*Δ and triple-*mep*Δ *At*AKT1, showed ^{15}N depletion compared to the N source after ammonium acquisition, indicating that NH_4^+ was the main form transported under these conditions. The data further indicate that the increase of external NH_3 with increasing pH did not significantly contribute to N acquisition in none of these cell strains. *Ta*TIP2;1-expressing cells were able to grow at pH values of up to 8.0 (Fig. 2B), and their growth and N content increased as the external pH in the culture medium increased (Fig. 2, B and D). The $\delta^{15}N$ values decreased as the biomass and N content increased with external pH and therefore with the increasing external NH_3 concentration in the culture medium (fig. S3), reaching values of approximately −13 mUr, similar to those shown by *Sc*Mep-expressing cells (Fig. 2, E and F). This augmented ^{15}N depletion with increasing pH is likely due to the thermodynamic isotope effect occurring when the chemical equilibrium NH_4^+/NH_3 in solution is displaced toward NH_3. This indicates that the increase of external NH_3 derived from the increasing pH contributes significantly to N acquisition in *Ta*TIP2;1-expressing cells, indicating that the substrate acquired by *Ta*TIP2;1 is NH_3, and not NH_4^+, in line with a previous report (*19*).

We next addressed whether a point mutation in the pore of *Sc*Mep2 previously shown to alter the kinetics of substrate translocation could also influence the $\delta^{15}N$ response. We used the *Sc*Mep2^{H194E} protein, in which a conserved histidine (His) residue (H194E) in the pore region is replaced by glutamate (*21*). Consistent with previous studies, similar to *Sc*Mep2, *Sc*Mep2^{H194E} restored the growth defect of triple-*mep*Δ cells grown on 1 mM ammonium (Figs. 1B and 2) (*21*). Thus, the *Sc*Mep2^{H194E} variant maintained transport activity, confirming that the conserved His residue at position 194 is not indispensable for the transport function of *Sc*Mep2 (*21*). Although cells expressing the *Sc*Mep2 and *Sc*Mep2^{H194E} showed similar $\delta^{15}N$ responses to pH, cells expressing the mutated protein always exhibited lower $\delta^{15}N$ values (Fig. 2E). These observations indicate that the protein structure influences the ability of *Sc*Mep2 to fractionate between ^{14}N and ^{15}N isotopes during ammonium transport.

Ammonium transport via *Sc*Meps can enable intracellular alkalinization in metabolically starved cells

We used an experimental setup, complementary to the IRMS technique described above, that could enable one to evidence an NH_3 translocation via *Sc*Mep proteins. Stopped-flow fluorescence spectroscopy allows one to follow changes in intracellular pH in response to

NH_3 or NH_4^+ uptake by monitoring fluorescence variations of the pH-sensitive probe 5-carboxyfluorescein diacetate (CFDA). To avoid a contribution of H^+ extrusion systems in the interpretations, we used metabolically starved cells, glucose-depleted and adenosine 5′-triphosphate (ATP)–exhausted, formerly grown with 76 mM ammonium and loaded with CFDA. Metabolically starved cells were suddenly exposed to an external concentration of 25 mM NH_4Cl (pH 8 and 23°C) before internal pH changes were recorded over time (Fig. 3A). We used these conditions of concentration and pH to apply an NH_3 gradient toward cytosol (*22*). As indicated by an increase in the intensity of carboxyfluorescein (CF) fluorescence, the addition of NH_4Cl to the external medium induced intracellular alkalinization, which indicated NH_3 transport in all tested strains. All strains containing *Sc*Mep proteins showed an instantaneous increase in fluorescence intensity and a plateau (pH alkalinization) after exposure to external ammonium. Only the triple-*mep*Δ strain displayed a linear time-dependent increase in fluorescence intensity (Fig. 3A). Because the yeast cells were metabolically inactive, these observations indicate that changes in internal pH are caused by the internal consumption of H^+ associated with NH_3 entrance and were unlikely due to active extrusion of H^+ from the cytoplasm. The weak alkalinization observed in the triple-*mep*Δ cells most likely reflected the diffusion of NH_3 through the cell membrane at pH 8 and 23°C. A slow and passive diffusion of NH_3 through the lipid bilayer, as observed in the triple-*mep*Δ strain, and an involvement of *Sc*Mep proteins in the transport of NH_3 with subsequent cytoplasmic alkalinization were supported by calculating the activation energy (E_a) of NH_3 transport. In the Arrhenius plot shown in Fig. 3B, diffusion of NH_3 through the lipid bilayer mediated by the triple-*mep*Δ cells (E_a = 38.0 ± 2.5 kcal mol^{-1}) exhibited a greater temperature dependence than transport occurring in the presence of *Sc*Mep proteins (E_a = 23.4 ± 1.3 kcal mol^{-1} for the wild-type cells and E_a = 8.76 ± 0.75, 12.43 ± 0.64, and 14.68 ± 1.35 kcal mol^{-1} for the triple-*mep*Δ cells expressing *Sc*Mep1, *Sc*Mep2, and *Sc*Mep3, respectively). These data indicate that the presence of *Sc*Mep proteins favors NH_3 translocation in metabolically starved cells.

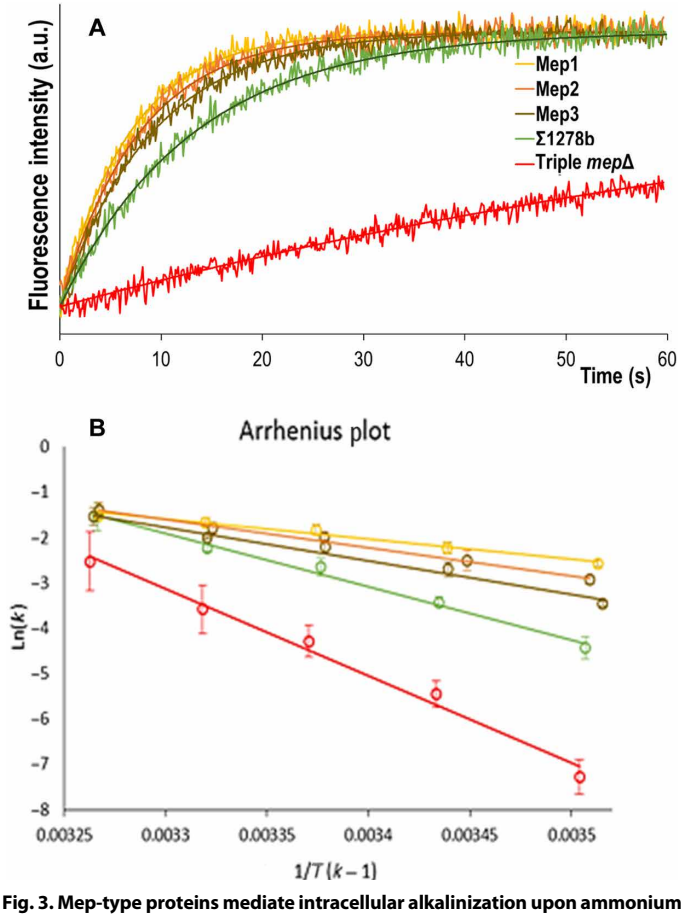

Fig. 3. Mep-type proteins mediate intracellular alkalinization upon ammonium uptake. Stopped-flow fluorescence signals obtained for intact triple-*mep*Δ (31019b) cells transformed with YCpMep1, YCpMep2, or YCpMep3 were compared with the negative control (31019b) and wild-type strain (Σ1278b). (**A**) Intracellular alkalinization was indicated by an increase in the fluorescence intensity resulting from the addition of 25 mM NH_4Cl (pH 8.0) to the external medium at t_0 = 23°C. (**B**) Arrhenius plot displaying the ln(*k*) of the changes in intracellular pH resulting from the transport of NH_3 as a function of the inverse of the temperature. Data are presented as means ± SE (n = 3).

^{15}N-depletion during uptake is a general feature of AMT-Mep-Rh proteins

We used yeast triple-*mep*Δ cells to heterologously express ammonium permeases belonging to the AMT-Mep-Rh protein family from different organisms (bacteria, fungi, green algae, plants, and animals) to test whether cellular ^{15}N depletion was only associated with yeast *Sc*Mep proteins or to a general feature of members of the AMT-Mep-Rh protein family. At high and low external ammonium supplies, growth of all AMT, Mep, or Rh protein–expressing cells was associated with ^{15}N depletion (Fig. 4), indicating that ^{15}N depletion is a general feature of members of AMT-Mep-Rh proteins. Again, expression of the potassium channel *At*AKT1 from *A. thaliana* in the triple-*mep*Δ strain did not lead to ^{15}N depletion at high ammonium concentrations (Fig. 4A). Our data (not shown) indicate that a concentration of at least 1 mM ammonium is required to observe the function of *At*AKT1 in triple-*mep*Δ cells and that, under these conditions, growth is not associated with ^{15}N depletion, indicating that NH_4^+ is transported. Expression of the tonoplast intrinsic protein *Ta*TIP2;1 from *T. aestivum* (*19*) favored growth at high ammonium and was associated with cellular ^{15}N depletion (Fig. 4A).

Using natural δ^{15}N to distinguish between different ammonium transport mechanisms in vivo

^{15}N depletion in yeast cells depended on the expression of functional *Sc*Mep proteins and was observed at low and high ammonium concentrations (Fig. 1), suggesting that *Sc*Meps were active under both conditions. At high ammonium concentrations, ammonium is also transported in a *Sc*Mep-independent manner, which was not associated with cellular ^{15}N depletion (Fig. 5). The latter ammonium transport process could occur via nonspecific cation channels (NSCCs). However, the molecular nature of these NSCC proteins remains unknown (*23*). When transported through NSCC, ammonium tends to compete with K^+ (*4*). We used a described inhibitor of the function of NSC1-type channels, hygromycin B (*23*), to distinguish different ammonium transport mechanisms, that is, *Sc*Mep-dependent and *Sc*Mep-independent mechanisms, and track the function of *Sc*Mep proteins at high ammonium concentrations. The no-interaction term *Sc*Mep × hygromycin B on cell growth supports the idea that hygromycin B does not interfere with *Sc*Mep (table S2). The wild-type and triple-*mep*Δ cells were grown in the presence of 13 mM K^+ and 76 mM ammonium at pH 4.3, conditions that are commonly used

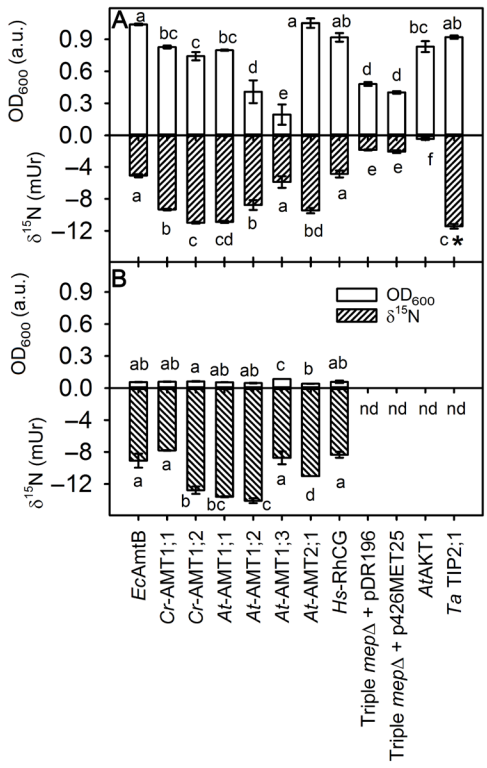

Fig. 4. Functional AMT-Rh protein superfamily depletes cells in ^{15}N. Isotopic N signature of triple-*mep*Δ (31019b) cells transformed with different AMT-Rh subfamily transporters from protista, eubacteria, plants, and animals. Yeast growth (top) and natural N isotope abundance (bottom) of different yeast strains grown at pH 4.3 in the presence of 13 mM K^+ and 76 mM NH_4^+ (**A**) or 0.5 mM NH_4^+ (**B**). **Ta*TIP2;1-containing cells were grown at pH 7.0. AMT-Rh carrier-containing strains grown in the presence of 76 mM NH_4^+ were compared with their respective negative control strains (31019b + pDR196 and 31019b + p426MET25) and other putative carriers of NH_4^+ (such as *At*AKT1 from *A. thaliana*) or NH_3 (such as *Ta*TIP2;1), which are not members of the AMT-Mep-Rh family, as controls. Control strains did not show growth in the presence of 0.5 mM NH_4^+. *Ec*AmtB (AMT from *Escherichia coli*), triple *mep*Δ + *Ec*AmtB; *Cr*-AMT1;1 (Amt1;1 from *Chlamydomonas reinhardtii*), triple *mep*Δ + *Cr*Amt1;1; *Cr*-AMT1;2 (AMT1;2 from *C. reinhardtii*), triple *mep*Δ + *Cr*AMT1;2; *At*-AMT1;1 (AMT1;1 from *A. thaliana*), triple *mep*Δ + *At*AMT1;1; *At*-AMT1;2 (AMT1;2 from *A. thaliana*), triple *mep*Δ + *At*AMT1;2; *At*-AMT1;3 (AMT1;3 from *A. thaliana*), triple *mep*Δ + *At*AMT1;3; *At*-AMT2;1 (AMT2;1 from *A. thaliana*), triple *mep*Δ + *At*AMT2;1; *Hs*-RhCG (RhCG from *Homo sapiens*), triple *mep*Δ + *Hs*RhCG. Data are presented as means ± SE ($n \geq 3$). Letters represent significant differences ($P \leq 0.05$). $\delta^{15}N$ of $(NH_4)_2SO_4$, −0.8 to 0.1 mUr. nd, not determined.

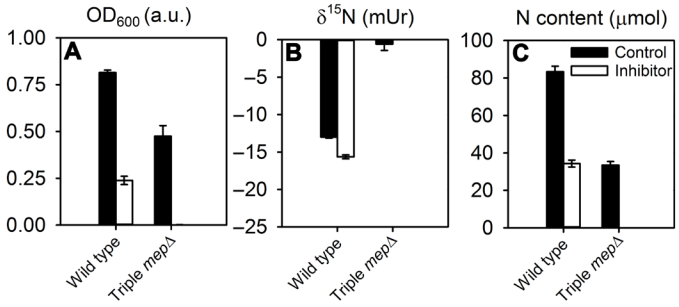

Fig. 5. Inhibition of NSC1-type channels does not affect cellular ^{15}N depletion. Inhibition of NSC1-type channels with hygromycin B in wild-type (Σ1278b) and triple-*mep*Δ (31019b) cells grown in the presence of 13 mM K^+ and 76 mM ammonium. (**A**) Yeast growth (OD_{600}), (**B**) natural N isotopic abundance (in milliUreys), and (**C**) total N content (in micromoles) in wild-type and triple-*mep*Δ yeast grown under control conditions (black bars) or in the presence of 300 μM hygromycin B, the NSCC type 1 inhibitor (white bars), at the end of the growth period. Yeast cells were grown for 48 hours at 185 rpm, 30°C, and pH 4.3. Data are presented as means ± SE ($n = 3$). $\delta^{15}N$ of $(NH_4)_2SO_4$, 0.0 mUr.

in minimal yeast medium (Fig. 5) (*4*). The triple-*mep*Δ cells showed weaker growth associated with almost no ^{15}N depletion (Figs. 1 and 5). However, in the presence of 300 μM hygromycin B, there was no growth of the triple-*mep*Δ cells (Fig. 5A), and cells were not able to accumulate N any longer (Fig. 5C). In contrast, the wild-type cells displayed reduced growth, along with a similar reduction in total N content (Fig. 5, A and C). Hygromycin B application to the wild-type strain preserved cellular ^{15}N depletion (Fig. 5B). This indicates that at high external ammonium concentrations, only *Sc*Mep-mediated ammonium transport was associated with significant ^{15}N depletion (Fig. 5B), whereas ammonium transport through NSC1-type channels showed no N isotope discrimination (Fig. 5 and fig. S1C, top).

Using natural $\delta^{15}N$ to address K^+/NH_4^+ interdependence, ammonium toxicity, and associated amino acid excretion

Following the identification of the two major functional components of ammonium transport at high substrate concentrations under the growth conditions tested, that is, NSC1-type channels and *Sc*Mep proteins (Fig. 5), we altered K^+ availability to assess the relative contribution of each component to the total amount of N transported (*4*). Irrespective of the K^+ concentration in the growth medium (1.3, 6, or 13 mM), wild-type cells were able to grow in the presence of any ammonium concentration (0.5 to 300 mM), whereas triple-*mep*Δ cells were able to grow only in the presence of ammonium concentrations greater than 5 mM (Fig. 6). As expected, decreasing the K^+ concentration in the growth medium from 13 to 1.3 mM decreased growth. At low ammonium concentrations, the growth of wild-type cells, but not of triple-*mep*Δ cells, was associated with ^{15}N depletion of the cells. Notably, cells became enriched with ^{15}N when wild-type or triple-*mep*Δ cells were grown in the presence of high ammonium and low K^+ concentrations (Fig. 6, C and G). This may be related to extrusion of N compounds enriched in ^{14}N, such as amino acids (*4*, *24*). We consistently detected higher amino acid concentrations in the external medium along with growth of both wild-type and triple-*mep*Δ cells at high ammonium and low K^+ concentrations (Fig. 6, C and G, and fig. S4).

At each K^+ concentration, cell ^{15}N depletion tended to increase with rising external ammonium until cell growth started to decrease, at which point ^{15}N depletion also started to decrease, reflecting ammonium toxicity (Fig. 6 and table S3). The interaction term between both factors, K^+ and NH_4^+ availabilities, on cell growth, isotopic composition, extracellular excretion of amino acids, and cell N content shows the strong dependence of these parameters on the ratio of external K^+/NH_4^+ concentrations (table S3). Our data illustrate how measurements of $\delta^{15}N$ can enable one to address K^+/NH_4^+ interdependence during growth, ammonium toxicity, and its associated amino acid excretion, the latter being inferred by cells' ^{15}N enrichment at high, toxic, ammonium concentrations.

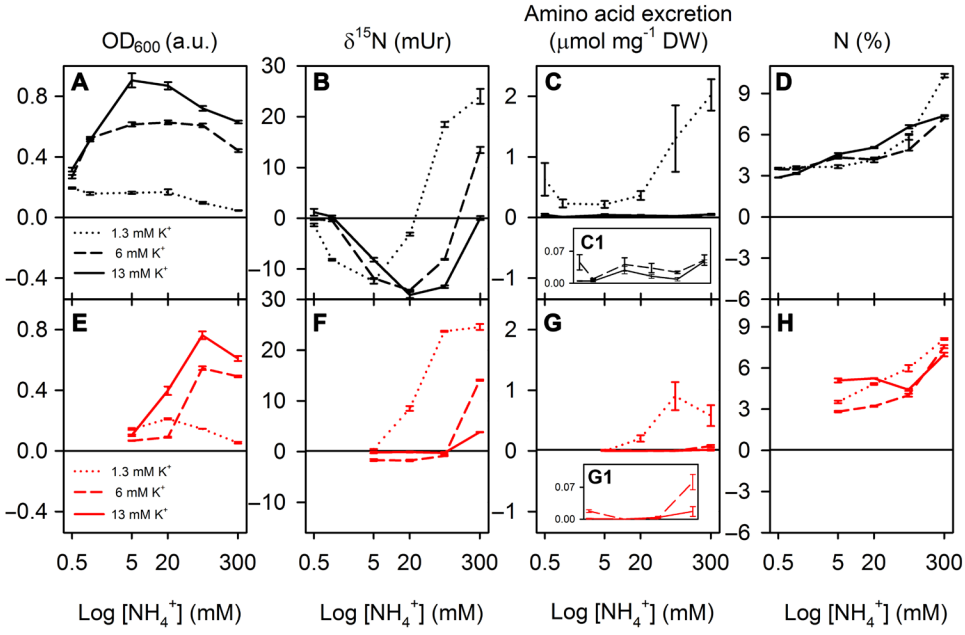

Fig. 6. External ammonium/potassium ratio affects cellular $\delta^{15}N$. Tracking $\delta^{15}N$ values in the presence of different external ammonium and potassium concentrations in *S. cerevisiae* (**A** to **D**) wild-type (Σ1278b; black) and (**E** to **H**) triple-*mep*Δ (31019b; red) strains. (A and E) Yeast growth (OD_{600}). (B and F) Yeast $\delta^{15}N$ (in milliUreys). (C and G) Amino acid concentrations detected in the media after yeast growth (μmol g^{-1} DW). (D and H) Yeast N content (%). Yeast cells were grown for 48 hours at 185 rpm, 30°C, and pH 4.3. Data are presented as means ± SE ($n = 3$). $\delta^{15}N$ of $(NH_4)_2SO_4$, 0.0 to 0.044 mUr. DW, dry weight.

DISCUSSION

Here, we show that the use of the natural N isotopic signature allows one to distinguish different functional ammonium transport mechanisms in vivo in yeast cells. At low ammonium concentrations (<5 mM, pH 4.3), the main proteins responsible for ammonium uptake are AMT-Mep-Rh–type proteins, whose N transport mechanism is associated with cellular ^{15}N depletion relative to the N source. However, at higher ammonium concentrations (>5 mM, pH 4.3), further transport systems contribute to and dominate ammonium uptake, which are not related to cellular ^{15}N depletion and likely reflect the activity of NSCCs (*23*). Because the $\delta^{15}N$ value of a total organism, like a yeast cell, is composed of the $\delta^{15}N$ values of a wide range of organic and inorganic compounds with quite different isotope characteristics including residual nonreduced N, amino acids, or nucleotides (*25*), the low level of ^{15}N depletion that is observed in the triple-*mep*Δ cells exposed to ammonium (Figs. 1 to 6) makes these cells a true negative control for studying *Sc*Mep-related ammonium transport mechanisms.

The slightly negative $\delta^{15}N$ values displayed by the triple-*mep*Δ strain when it was exposed to high ammonium (Figs. 1 and 5) may be the combined outcome of NH_3 diffusion through the lipid bilayer and a metabolic effect. However, the almost constant and highly negative $\delta^{15}N$ values displayed by *Sc*Mep-expressing yeast cells grown in the presence of low (1 mM) and high (76 mM) ammonium concentrations in this study may be considered an independent event from the inherent interfering and overlapping fractionation processes linked to N metabolism. When fractionation processes linked to N metabolism interfere with the total cellular biomass $\delta^{15}N$ value, the $\delta^{15}N$ value changes in a manner dependent on factors like K^+ availability and extracellular excretion of ^{15}N-depleted organic compounds, such as amino acids (Fig. 6 and fig. S4; see below).

^{15}N depletion supports deprotonation during transport through AMT-Mep-Rh proteins in yeast cells

In solution, NH_4^+ and NH_3 are in equilibrium. Because of the equilibrium isotope effect on the deprotonation of NH_4^+ into $NH_3 + H^+$, the heavier isotope is discriminated at a rate of ≈−44.3 mUr (*17*). At high NH_4^+ concentrations, when at least one of the *Sc*Mep proteins was expressed in yeast, cells became ^{15}N-depleted relative to the N source (Fig. 1). Thus, NH_3 is involved in the ammonium transport process mediated by *Sc*Mep proteins. The depletion of ^{15}N in yeast cells due to ammonium transport through *Sc*Mep proteins may be due to the following mechanisms (fig. S1): (i) the recruitment of NH_3 in solution, (ii) preferential recruitment of $^{14}NH_4^+$ versus $^{15}NH_4^+$ in solution followed by nondiscriminating NH_4^+ transport, or (iii) recruitment of NH_4^+ followed by deprotonation of NH_4^+ into NH_3 and H^+ before transport through the pore.

Recruitment of NH_3 in solution

If *Sc*Mep proteins recruit NH_3 in solution, then the cellular $\delta^{15}N$ value is expected to decrease with increasing pH because the NH_3 concentration increases exponentially with pH (fig. S3). However, *Sc*Mep-expressing cells showed an opposite trend, as cellular $\delta^{15}N$ values increased with increasing pH (Fig. 2). NH_3 is therefore not likely to be the chemical species recruited by *Sc*Meps, which is consistent with the mechanism suggested for *Ec*AmtB and other members of the AMT-Mep-Rh family (*11*, *12*, *15*, *26*). The thermodynamic isotope effect linked to NH_4^+/NH_3 equilibrium in the external solution appears not to be the origin of the ^{15}N depletion of Mep-expressing yeast cells. In contrast, a slight decrease in $\delta^{15}N$ values was observed in the triple-*mep*Δ cells, which passively permeate NH_3 through the lipid bilayer (Figs. 2 and 3), while a larger decrease was observed in *Ta*TIP2;1-expressing yeast cells (Fig. 2). *Ta*TIP2;1, whose ability to transport ammonium is mainly driven by the transmembrane NH_3 concentration gradient,

directly recruits and transports NH_3 from the external solution (Fig. 2) (*9*, *19*).

Preferential recruitment of $^{14}NH_4^+$ versus $^{15}NH_4^+$ in solution

On the basis of the crystal structure of *Ec*AmtB and modeling of substrate–amino acid interactions, it has been proposed that *Ec*AmtB recruits NH_4^+ rather than NH_3 at its outer vestibule (*15*). Moreover, the predominance of NH_4^+ over NH_3 in solution would render NH_4^+ recruitment by *Sc*Mep proteins more efficient. Because of its lower mass, ^{14}N is more energetic than the ^{15}N isotope and has a higher probability of reacting (*27*); therefore, $^{14}NH_4^+$ may putatively be recruited faster than $^{15}NH_4^+$ in the external vestibule of ScMep proteins. However, when a kinetic isotope effect occurs, mass transfer or bonding changes must occur during the process or reaction (*16*). For this reason, the simple preferential recruitment of $^{14}NH_4^+$ versus $^{15}NH_4^+$ in solution by Mep-type proteins is not expected to be the major factor determining the ^{15}N depletion in Mep-expressing cells. The NH_4^+ recruited must experience changes in its molecule to give an isotopic fractionation linked to a kinetic effect. In this way, this fractionation must be related to the transformation, that is, dissociation of the molecule during the transport process through the protein.

Recruitment of NH_4^+ followed by deprotonation

When grown on ammonium, ^{15}N depletion may be related to a kinetic isotope effect associated with different dissociation rates of both isotopologues (*16*). The assays performed with the triple-*mep*Δ cells expressing *Sc*Mep2^{H194E} provided support for this assumption because they showed that (i) the conserved His residue at position H194 was not indispensable for the transport function of *Sc*Mep2 (*21*) or fractionation mechanism (Figs. 1 and 2) and (ii) the structure of the molecule was involved in the isotope fractionation process (Figs. 1 and 2). These results are compatible with the hypothesis that *Sc*Mep2 recruits NH_4^+, which is then deprotonated in the core of the *Sc*Mep molecule (*21*, *26*). The H194E mutation has been shown to modify the transport kinetics of *Sc*Mep2, leading to a reduced affinity and an increased substrate transport rate (*21*). The stronger ^{15}N depletion observed in *Sc*Mep2^{H194E}-expressing cells compared to cells expressing *Sc*Mep*2* indicated that the protein structure is involved in the isotopic fractionation of *Sc*Mep*2*, a kinetic isotope effect, and therefore in the NH_4^+ deprotonation event (Fig. 1).

The stopped-flow experiments we designed with metabolically starved cells suggest that *Sc*Meps are capable of translocating NH_3 (Fig. 3), further supporting the NH_4^+ deprotonation model. However, the observed cytoplasmic alkalization associated with NH_4^+ deprotonation does not exclude the fact that the transport may be electrogenic (cotransport of NH_3 and H^+) in metabolically active cells, as has previously been shown for plant AMT1-type proteins (*9*, *13*). The yeast cells were metabolically starved in our experimental setup. Moreover, it has been proposed that the timing of H^+ and NH_3 transport via AMT-Mep proteins through the membrane may be different (*28*). Therefore, while the ^{15}N isotope fractionation evidences the ammonium deprotonation process, electrophysiology studies are required to elucidate whether *Sc*Meps perform electrogenic or electroneutral transport.

Several studies have reported the regulated inhibition, at the transcriptional level and/or at the transport activity level, of ammonium transport through AMT-Mep-Rh proteins by elevated ammonium concentrations in yeast (*18*, *29*, *30*), bacteria (*31*), and plants (*32*). However, our data indicate that some activity of AMT-Mep-Rh proteins, either endogenous or heterologous, is conserved at high ammonium concentrations in yeast cells. Regulatory mechanisms present in the original cells most likely do not function when plant and animal proteins are heterologously expressed in yeast. In the case of the wild-type yeast strain (Fig. 1), *Sc*Meps, or at least one of the three, were not totally inhibited, showing an activity responsible for the discrimination observed in the presence of 76 mM ammonium, and the inhibition of the NSC1-type channels with hygromycin B did not affect $\delta^{15}N$ values (Fig. 5). In agreement with these results, Feller *et al.* (*33*) showed a reduction in the growth of triple-*mep*Δ cells at 20 mM and even at 80 mM ammonium in relation to that shown by wild-type cells grown on yeast nitrogen base medium, which is also visible in this study (Figs. 2 and 6). The *Sc*Mep2-mediated transport at low pH, below 4, appears sufficient to ensure growth at 76 mM ammonium (Fig. 2). Marini *et al.* (*18*), using a specific minimal buffered medium with different N sources, showed that all three *MEP* genes are submitted to N catabolite repression and thus repressed when cells were provided with a high ammonium concentration compared to cells grown on nonpreferred N sources such as proline. However, *MEP* expression was not totally shut down on high ammonium. LacZ data showed that all three *MEP* genes are still expressed, although at reduced levels, on high ammonium concentrations and that the maximal repression was only achieved when glutamine was combined with ammonium (*18*). Our results support the idea that the reduced level of *Sc*Mep proteins produced at high ammonium concentrations contributes to ammonium transport and growth under these conditions.

$\delta^{15}N$ allows differentiating between different ammonium transport mechanisms in vivo and highlights excretion of amino acids (^{15}N-depleted compounds) in yeasts under ammonium toxicity

Excess uptake of ammonium causes toxicity in plants, animals, and microorganisms (*1*, *4*, *7*). The similarities between the physicochemical properties of K^+ and NH_4^+ in solution in terms of charge, radius, and hydration energies support the hypothesis that large amounts of NH_4^+ might enter the cells via NSCCs, particularly when external K^+ concentrations are low (*4*, *23*). In addition, experiments in yeast with different combinations of external NH_4^+/K^+ ratios showed a nexus between concentrations of NH_4^+ and K^+ in the growth medium (table S3). For instance, for each considered external K^+ concentration, cellular $\delta^{15}N$ values, growth, and amino acids in the culture media highlighted the fact that yeast cells experiencing ammonium toxicity excreted amino acids (Fig. 6 and fig. S4). Some important metabolic processes and reactions, such as primary N assimilation by glutamine synthetase, amidation, and/or transamination, discriminate against the heavier N isotope, leading to ^{15}N depletion from organic compound products and the subsequent enrichment of ^{15}N in the remaining unassimilated substrates (*24*). Similar responses to K^+/NH_4^+ imbalances have also been observed in plants (*20*) and animals (*1*) and account for cellular ^{15}N enrichment at low K^+/NH_4^+ ratios.

CONCLUSIONS AND BIOLOGICAL RELEVANCE

Here, on the basis of N isotope discrimination associated with ammonium transport by *Sc*Meps at distinct pH, we showed that (i) NH_4^+, and not NH_3, is most likely the chemical species recruited by *Sc*Mep proteins and (ii) the transport of NH_4^+ by AMT-Mep-Rh proteins is associated with NH_4^+ deprotonation, which confers specificity for NH_4^+ transport. In view of the physical-chemical similarities

between NH_4^+ and K^+, the NH_4^+ deprotonation process may be a mechanistic feature conferring selectivity against K^+ and for NH_3 transport after NH_4^+ recruitment. If deprotonation occurring inside the AMT-Mep-Rh protein is the step providing selectivity for NH_4^+ transport, then mutations in the pore that allow the transport of other ions such as K^+ may be identified. A recent study by Hall and Yan (*34*) reveals that mutations in the twin His residues in the *Ec*AmtB central pore allow the K^+ translocation against a concentration gradient. Notably, human Rh-associated glycoprotein variants associated with overhydrated spherostomatocytosis were reported to mediate K^+ transport (*35*). The link between NH_4^+ deprotonation within AMT-Mep-Rh proteins and their specificity for NH_4^+ transport may be a central common feature in this large, widespread family of transporters present across all life domains. We propose that this deprotonation step is independent of the net transport of NH_3 (electroneutral transport) or $NH_3 + H^+$ (electrogenic transport) through the protein (fig. S1B). The natural N isotope fractionation method presented here will become complementary to net charge movement assessment and 3D structure to achieve a precise characterization of the mechanism of ammonium transport for each considered ammonium membrane transport protein. These findings provide new insights into the controversy surrounding ammonium transport systems and mechanisms, leading to a unifying hypothesis for ammonium transport in living organisms.

MATERIALS AND METHODS

Strains and growth conditions

The *S. cerevisiae* strains used in this study were all isogenic with the wild-type Σ1278b, with the exception of the mutations and transformations specified throughout the text (plasmids used in this study are listed in table S4). All cultures were started with an initial inoculum of $\approx 10^4$ cells ml^{-1}. Cells were grown in minimal medium [$CaCl_2$ $2H_2O$ (0.1 g $liter^{-1}$), NaCl (0.1 g $liter^{-1}$), $MgSO_4$ $7H_2O$ (0.5 g $liter^{-1}$), boric acid (0.5 mg $liter^{-1}$), $CuSO_4$ $5H_2O$ (0.04 mg $liter^{-1}$), KI (0.1 mg $liter^{-1}$), $FeCl_3$ $6H_2O$ (0.2 mg $liter^{-1}$), $MnSO_4$ H_2O (0.4 mg $liter^{-1}$), sodium molybdate $2H_2O$ (0.2 mg $liter^{-1}$), biotin (10^{-3} mg $liter^{-1}$), calcium pantothenate (0.2 mg $liter^{-1}$), folic acid (10^{-3} mg $liter^{-1}$), inositol (1 mg $liter^{-1}$), nicotinic acid (0.2 mg $liter^{-1}$), *p*-aminobenzoic acid (0.1 mg $liter^{-1}$), pyridoxine HCl (0.2 mg $liter^{-1}$), riboflavin (0.1 mg $liter^{-1}$), thiamine HCl (0.2 mg $liter^{-1}$), and $ZnSO_4$ (0.4 mg $liter^{-1}$) (pH 4.3)] with 0.5% glucose as the carbon source (*4*). Adjustments to the pH in some experiments (with NaOH) are indicated in the text and figure captions. Nitrogen and potassium sources were added to this minimal medium as specified in the text and figures. Various concentrations of $(NH_4)_2SO_4$ were added as a nitrogen source (ranging from 0.5 to 300; concentrations specified for each experiment/figure). The K^+ concentrations (1.3, 6, and 13 mM K^+) used in the experiments were prepared from a stock solution of 1.3 M K^+ [KCl (98 g $liter^{-1}$) and KH_2PO_4 (2 g $liter^{-1}$)] (*4*). For tests requiring NSC1-type channel blockers, hygromycin B was added to the minimal medium at 300 μM (*23*). The *Ta*TIP2;1-containing yeast strain with a Gal promoter was grown in the presence of galactose (3%) as the C source instead of glucose (0.5%). In this case, because of its scarce complementation at pH values below 6.5, the culture media for the *Ta*TIP2;1-containing yeast strain with a Gal promoter were adjusted to higher pH values (6.5, 7, and 8) (*19*). The triple-*mep*Δ yeast strain (31019b) was also grown on galactose 3% as the C source instead of glucose (0.5%) in this experiment (pH 6.5, 7, and 8). Thus, the final culture media formulations were sterilized by filtration using a sterile Corning 250-ml vacuum filter/storage bottle system with a 0.22-μm pore and polyethersulfone membrane (Corning Incorporated) to avoid unwanted reactions during the thermal sterilization process (autoclave). The triple mutant strain used in this study, 31019b (triple *mep*Δ), is deficient in ammonium permeases (yeast *Sc*Mep proteins) and was therefore expected to be the ideal strain for analyzing the transport of NH_3/NH_4^+ mediated by heterologously expressed ammonium carriers (*18*).

Isotopic N composition, isotope effect estimation, and N content

Yeast cells were grown under the specified conditions for each experiment (see the text and figure captions), then collected by centrifugation (for 15 min at 5000*g* and 20°C), and washed at least twice with autoclaved Milli-Q water. After centrifugation (for 15 min at 5000*g* and 20°C), the pellets were frozen at −80°C and freeze-dried before the isotope determinations. Freeze-dried material was also weighed to record the biomass. The supernatants from yeast cells collected in some experiments were frozen at −80°C until further analysis (see the "Determination of amino acid contents in the external culture medium" section).

Approximately 0.5 to 1 mg of freeze-dried yeast material from each sample was separately packed in tin capsules. The $^{15}N/^{14}N$ ratios of the samples were determined by continuous-flow IRMS (*36*) using an Isoprime (GV Instruments) stable IRMS coupled to a EuroEA (EuroVector) elemental analyzer for online sample preparation via Dumas combustion. The standards used in this study were IAEA-N1 and USGS-35, and $\delta^{15}N$ results were normalized to air. The precision of the isotope-ratio analysis, which was calculated using values obtained from six to nine replicates from laboratory standard materials interspersed among samples from every batch analysis, was ≤0.2 mUr. The results of the analysis of the N isotope composition are expressed as $\delta^{15}N$ (in milliUreys) normalized to atmospheric N_2 and were calculated using the following equation: $\delta^{15}N$ (in Ureys) = $(R_{sample}/R_{standard}) - 1$, where R_{sample} is the $^{15}N/^{14}N$ ratio of the sample and $R_{standard}$ is the $^{15}N/^{14}N$ ratio of atmospheric N_2.

This approach has the following advantages over other previously used methods: (i) It integrates the N taken up over time in vivo, not only over a short timeframe (seconds), which is used by most electrophysiological approaches conducted in vitro (not during the growth period); (ii) it allows the amounts of N taken up as NH_3 (or NH_3/H^+) or NH_4^+ to be estimated when both forms are taken up simultaneously; (iii) it is a direct determination of the N concentration (not indirectly, as in measures of parallel events such as pH change or uptake of an analog, that is, methylammonium); and (iv) it is not intrusive. However, the two main limitations are as follows: (i) Unlimited and steady-state ammonium and potassium conditions are required to obtain clear evidence of NH_4^+ deprotonation, and (ii) additional and complementary techniques, such as net charge movement assessment and 3D-structure, are required to discern whether NH_3 or $NH_3 + H^+$ is being transported.

Stopped-flow fluorescence assays

Stopped-flow assays were based on the methods reported by Bertl and Kaldenhoff (*22*), with some modifications. Briefly, cells were grown in the minimal medium described above in the presence of 76 mM ammonium and 13 mM K^+ on an orbital shaker at 185 rpm and 30°C up to an $OD_{600} < 1$. Yeast cells were harvested by centrifugation

(for 15 min at 5000*g* and 20°C), washed (×2), resuspended in loading buffer [50 mM Hepes and NaOH (pH 5.7); wet weight, 3 ml g^{-1}], and incubated for at least 1 hour on ice (to ensure complete glucose depletion and ATP exhaustion, which represents metabolic starvation). Cells were then preloaded (15 min at 30°C) with the membrane-permeable nonfluorescent dye CFDA (1 mM), which was hydrolyzed after entering the cell, releasing the membrane-impermeable fluorescent form CF. Finally, 1 ml of this cell suspension was centrifuged (for 10 min at 5000*g* and 4°C), resuspended in 10 ml of ice-cold incubation buffer [50 mM NaCl and 10 mM tris-HCl (pH 8)], and maintained on ice until assay.

Transport experiments were performed in a stopped-flow spectrophotometer (Hi-TECH Scientific PQ/SF-53) at a controlled temperature with 2 ms of dead time using a 470-nm excitation filter and a >530-nm cutoff filter. Experiments were performed at various temperatures. For each experimental condition, four to six runs were usually stored and analyzed. Intact yeast cells equilibrated in incubation buffer were mixed with an equal volume of test solution [50 mM NH_4Cl and 10 mM tris-HCl (pH 8)] with the same osmolarity (preventing volume changes due to osmotic fluxes that could interfere with the signal) but a different ionic composition (50 mM NH_4Cl instead of 50 mM NaCl) to measure NH_3/NH_4^+ transport, resulting in an inwardly directed 25 mM NH_3/NH_4^+ gradient. NH_4^+ or NH_3 uptake induces a change in the intracellular pH that was monitored by measuring fluorescence intensity over time (*22*). The kinetic rate constant of the process (k) was estimated by fitting the signals to a single exponential function. The E_a of transport was evaluated from the slope of the Arrhenius plot [ln(k) as a function of $1/T$, where T is the temperature in kelvin] multiplied by the gas constant R. Three stopped-flow experiments were performed independently, and the results obtained from all of them were coincident with those shown in Fig. 3. For each experiment, yeast cells grown from three independent batches were blended. Each determination was replicated at least three times.

Determination of amino acid contents in the external culture medium

Following yeast growth, the culture medium was centrifuged (for 15 min at 5000*g* and 20°C) and then filtered (Ø = 20 μm). The soluble amino acid contents were then determined by high-performance capillary electrophoresis using a Beckman Coulter PA-800 apparatus (Beckman Coulter Inc.) with a laser-induced fluorescence detector (488 nm) equipped with a fused silica capillary (diameter, 50 μm; length, 43/53.2 cm) in an electrophoresis buffer containing 50 mM borax and 45 mM α-cyclodextrin at pH 9.2. Analyses were performed at 30 kV and 20°C. Known concentrations of norvaline and homoglutamic acid were added to all samples as internal references. The filtered supernatants were diluted (1:5) with 20 mM borate buffer (pH 10) and derivatized before detection with 1 mM fluorescein isothiocyanate in acetone. Gly + Ser contents were detected as a single peak.

Statistical analyses

All statistical analyses were performed with IBM SPSS for Windows (IBM). According to the number of independent factors considered for each experiment, one-way, two-way, or three-way analysis of variance was performed (see figures and tables for further information). F value in combination with P value was used to determine significant effects of factors (independent variables) on the parameters considered (dependent variables). Whole-model R^2 and interaction term effects between independent factors on each parameter have been presented in all tables of analysis of variance. All statistical analyses were conducted at a significance level of 5% ($P \leq 0.05$) and under normality and homoscedasticity assumption. In post hoc analysis tests, least significant difference statistics was used.

SUPPLEMENTARY MATERIALS

Supplementary material for this article is available at http://advances.sciencemag.org/cgi/content/full/4/9/eaar3599/DC1

Fig. S1. Ammonium transport mechanisms (fluxes) associated with charge movement.
Fig. S2. Growth and N content of the distinct yeast strains.
Fig. S3. Relative concentrations of NH_4^+ and NH_3 in solution expressed as a percentage of the total ammonium concentration ($NH_4^+ + NH_3$) as a function of solution pH.
Fig. S4. Amino acids excreted into the medium by wild-type (black bars) and triple-*mep*Δ (red bars) cells expressed as a percentage of the total amino acid pool (shown in Fig.6).
Table S1. Two-way analysis of variance of *Sc*Mep/NH_3 transporter presence and pH.
Table S2. Analysis of variance of *Sc*Mep presence and hygromycin B application.
Table S3. Three-way analysis of variance of *Sc*Mep presence and external potassium and ammonium availabilities.
Table S4. Plasmids used in this study.
References (*37*–*47*)

REFERENCES AND NOTES

1. I. D. Weiner, J. W. Verlander, Role of NH_3 and NH_4^+ transporters in renal acid-base transport. *Am. J. Physiol. Renal Physiol.* **300**, F11–F23 (2011).
2. J. B. Spinelli, H. Yoon, A. E. Ringel, S. Jeanfavre, C. B. Clish, M. C. Haigis, Metabolic recycling of ammonia via glutamate dehydrogenase supports breast cancer biomass. *Science* **358**, 941–946 (2017).
3. A. Merhi, P. Delrée, A. M. Marini, The metabolic waste ammonium regulates mTORC2 and mTORC1 signaling. *Sci. Rep.* **7**, 44602 (2017).
4. D. C. Hess, W. Lu, J. D. Rabinowitz, D. Botstein, Ammonium toxicity and potassium limitation in yeast. *PLOS Biol.* **4**, e351 (2006).
5. Y. N. Antonenko, P. Pohl, G. A. Denisov, Permeation of ammonia across bilayer lipid membranes studied by ammonium ion selective microelectrodes. *Biophys. J.* **72**, 2187–2195 (1997).
6. A. M. Marini, S. Vissers, A. Urrestarazu, B. André, Cloning and expression of the MEP1 gene encoding an ammonium transporter in *Saccharomyces cerevisiae*. *EMBO J.* **13**, 3456–3463 (1994).
7. O. Ninnemann, J.-C. Jauniaux, W. B. Frommer, Identification of a high affinity NH_4^+ transporter from plants. *EMBO J.* **13**, 3464–3471 (1994).
8. A.-M. Marini, A. Urrestarazu, R. Beauwens, B. André, The Rh (Rhesus) blood group polypeptides are related to NH_4^+ transporters. *Trends Biochem. Sci.* **22**, 460–461 (1997).
9. T. R. McDonald, J. M. Ward, Evolution of electrogenic ammonium transporters (AMTs). *Front. Plant Sci.* **7**, 352 (2016).
10. D. Lupo, X.-D. Li, A. Durand, T. Tomizaki, B. Cherif-Zahar, G. Matassi, M. Merrick, F. K. Winkler, The 1.3-Å resolution structure of *Nitrosomonas europaea* Rh50 and mechanistic implications for NH_3 transport by Rhesus family proteins. *Proc. Natl. Acad. Sci. U.S.A.* **104**, 19303–19308 (2007).
11. S. Khademi, J. O'Connell III, J. Remis, Y. Robles-Colmenares, L. J. W. Miercke, R. M. Stroud, Mechanism of ammonia transport by Amt/MEP/Rh: Structure of AmtB at 1.35 Å. *Science* **305**, 1587–1594 (2004).
12. L. Zheng, D. Kostrewa, S. Bernèche, F. K. Winkler, X.-D. Li, The mechanism of ammonia transport based on the crystal structure of AmtB of *Escherichia coli*. *Proc. Natl. Acad. Sci. U.S.A.* **101**, 17090–17095 (2004).
13. U. Ludewig, N. von Wirén, W. B. Frommer, Uniport of NH_4^+ by the root hair plasma membrane ammonium transporter LeAMT1;1. *J. Biol. Chem.* **277**, 13548–13555 (2002).
14. B. Neuhäuser, M. Dynowski, U. Ludewig, Channel-like NH_3 flux by ammonium transporter AtAMT2. *FEBS Lett.* **583**, 2833–2838 (2009).
15. U. Akgun, S. Khademi, Periplasmic vestibule plays an important role for solute recruitment, selectivity, and gating in the Rh/Amt/MEP superfamily. *Proc. Natl. Acad. Sci. U.S.A.* **108**, 3970–3975 (2011).
16. W. W. Cleland, The use of isotope effects to determine enzyme mechanisms. *Arch. Biochem. Biophys.* **433**, 2–12 (2005).
17. L. Li, B. S. Lollar, H. Li, U. G. Wortmann, G. Lacrampe-Couloume, Ammonium stability and nitrogen isotope fractionations for NH_4^+–NH_3(aq)–NH_3(gas) systems at 20–70°C and pH of 2–13: Applications to habitability and nitrogen cycling in low-temperature hydrothermal systems. *Geochim. Cosmochim. Acta* **84**, 280–296 (2012).

18. A.-M. Marini, S. Soussi-Boudekou, S. Vissers, B. Andre, A family of ammonium transporters in *Saccharomyces cerevisiae*. *Mol. Cell. Biol.* **17**, 4282–4293 (1997).
19. T. P. Jahn, A. L. B. Møller, T. Zeuthen, L. M. Holm, D. A. Klærke, B. Mohsin, W. Kühlbrandt, J. K. Schjoerring, Aquaporin homologues in plants and mammals transport ammonia. *FEBS Lett.* **574**, 31–36 (2004).
20. F. t. Hoopen, T. A. Cuin, P. Pedas, J. N. Hegelund, S. Shabala, J. K. Schjoerring, T. P. Jahn, Competition between uptake of ammonium and potassium in barley and *Arabidopsis* roots: Molecular mechanisms and physiological consequences. *J. Exp. Bot.* **61**, 2303–2315 (2010).
21. M. Boeckstaens, B. André, A. M. Marini, Distinct transport mechanisms in yeast ammonium transport/sensor proteins of the Mep/Amt/Rh family and impact on filamentation. *J. Biol. Chem.* **283**, 21362–21370 (2008).
22. A. Bertl, R. Kaldenhoff, Function of a separate NH_3-pore in Aquaporin TIP2;2 from wheat. *FEBS Lett.* **581**, 5413–5417 (2007).
23. H. Bihler, C. L. Slayman, A. Bertl, Low-affinity potassium uptake by *Saccharomyces cerevisiae* is mediated by NSC1, a calcium-blocked non-specific cation channel. *Biochim. Biophys. Acta* **1558**, 109–118 (2002).
24. R. A. Werner, H.-L. Schmidt, The in vivo nitrogen isotope discrimination among organic plant compounds. *Phytochemistry* **61**, 465–484 (2002).
25. H.-L. Schmidt, R. J. Robins, R. A. Werner, Multi-factorial in vivo stable isotope fractionation: Causes, correlations, consequences and applications. *Isotopes Environ. Health Stud.* **51**, 155–199 (2015).
26. A. M. Marini, M. Boeckstaens, F. Benjelloun, B. Chérif-Zahar, B. André, Structural involvement in substrate recognition of an essential aspartate residue conserved in Mep/Amt and Rh-type ammonium transporters. *Curr. Genet.* **49**, 364–374 (2006).
27. A. Mariotti, J. C. Germon, P. Hubert, P. Kaiser, R. Letolle, A. Tardieux, P. Tardieux, Experimental determination of nitrogen kinetic isotope fractionation: Some principles; illustration for the denitrification and nitrification processes. *Plant Soil* **62**, 413–430 (1981).
28. F. C. Boogerd, H. Ma, F. J. Bruggeman, W. C. van Heeswijk, R. García-Contreras, D. Molenaar, K. Krab, H. V. Westerhoff, AmtB-mediated NH_3 transport in prokaryotes must be active and as a consequence regulation of transport by GlnK is mandatory to limit futile cycling of NH_4^+/NH_3. *FEBS Lett.* **585**, 23–28 (2011).
29. M. Boeckstaens, E. Llinares, P. Van Vooren, A. M. Marini, The TORC1 effector kinase Npr1 fine tunes the inherent activity of the Mep2 ammonium transport protein. *Nat. Commun.* **5**, 3101 (2014).
30. M. Boeckstaens, A. Merhi, E. Llinares, P. Van Vooren, J.-Y. Springael, R. Wintjens, A. M. Marini, Identification of a novel regulatory mechanism of nutrient transport controlled by TORC1-Npr1-Amu1/Par32. *PLOS Genet.* **11**, e1005382 (2015).
31. G. Coutts, G. Thomas, D. Blakey, M. Merrick, Membrane sequestration of the signal transduction protein GlnK by the ammonium transporter AmtB. *EMBO J.* **21**, 536–545 (2002).
32. D. Loqué, S. Lalonde, L. L. Looger, N. von Wirén, W. B. Frommer, A cytosolic *trans*-activation domain essential for ammonium uptake. *Nature* **446**, 195–198 (2007).
33. A. Feller, M. Boeckstaens, A. M. Marini, E. Dubois, Transduction of the nitrogen signal activating Gln3-mediated transcription is independent of Npr1 kinase and Rsp5-Bul1/2 ubiquitin ligase in *Saccharomyces cerevisiae*. *J. Biol. Chem.* **281**, 28546–28554 (2006).
34. J. A. Hall, D. Yan, The molecular basis of K^+ exclusion by the *Escherichia coli* ammonium channel AmtB. *J. Biol. Chem.* **288**, 14080–14086 (2013).
35. L. J. Bruce, H. Guizouarn, N. M. Burton, N. Gabillat, J. Poole, J. F. Flatt, R. L. Brady, F. Borgese, J. Delaunay, G. W. Stewart, The monovalent cation leak in overhydrated stomatocytic red blood cells results from amino acid substitutions in the Rh-associated glycoprotein. *Blood* **113**, 1350–1357 (2009).
36. T. Preston, N. J. P. Owens, Interfacing an automatic elemental analyser with an isotope ratio mass spectrometer: The potential for fully automated total nitrogen and nitrogen-15 analysis. *Analyst* **108**, 971–977 (1983).
37. D. Mumberg, R. Müller, M. Funk, Regulatable promoters of *Saccharomyces cerevisiae*: Comparison of transcriptional activity and their use for heterologous expression. *Nucleic Acids Res.* **22**, 5767–5768 (1994).
38. L. Yuan, D. Loqué, S. Kojima, S. Rauch, K. Ishiyama, E. Inoue, H. Takahashi, N. von Wirén, The organization of high-affinity ammonium uptake in *Arabidopsis* roots depends on the spatial arrangement and biochemical properties of AMT1-type transporters. *Plant Cell* **19**, 2636–2652 (2007).
39. A. Javelle, G. Thomas, A.-M. Marini, R. Krämer, M. Merrick, In vivo functional characterization of the *Escherichia coli* ammonium channel AmtB: Evidence for metabolic coupling of AmtB to glutamine synthetase. *Biochem. J.* **390**, 215–222 (2005).
40. A. M. Marini, G. Matassi, V. Raynal, B. André, J.-P. Cartron, B. Chérif-Zahar, The human Rhesus-associated RhAG protein and a kidney homologue promote ammonium transport in yeast. *Nat. Genet.* **26**, 341–344 (2000).
41. D. Rentsch, M. Laloi, I. Rouhara, E. Schmelzer, S. Delrot, W. B. Frommer, *NTR1* encodes a high affinity oligopeptide transporter in *Arabidopsis*. *FEBS Lett.* **370**, 264–268 (1995).
42. L. Yuan, R. Gu, Y. Xuan, E. Smith-Valle, D. Loqué, W. B. Frommer, N. von Wirén, Allosteric regulation of transport activity by heterotrimerization of *Arabidopsis* ammonium transporter complexes in vivo. *Plant Cell* **25**, 974–984 (2013).
43. A. Meyer, S. Eskandari, S. Grallath, D. Rentsch, AtGAT1, a high affinity transporter for γ-aminobutyric acid in *Arabidopsis thaliana*. *J. Biol. Chem.* **281**, 7197–7204 (2006).
44. M. Minet, M.-E. Dufour, F. Lacroute, Complementation of *Saccharomyces cerevisiae* auxotrophic mutants by *Arabidopsis thaliana* cDNAs. *Plant J.* **2**, 417–422 (1992).
45. H. Sentenac, N. Bonneaud, M. Minet, F. Lacroute, J. M. Salmon, F. Gaymard, C. Grignon, Cloning and expression in yeast of a plant potassium ion transport system. *Science* **256**, 663–665 (1992).
46. D. P. Schachtman, J. I. Schroeder, Structure and transport mechanism of a high-affinity potassium uptake transporter from higher plants. *Nature* **370**, 655–658 (1994).
47. N. Bonneaud, O. Ozier-Kalogeropoulos, G. Li, M. Labouesse, L. Minvielle-Sebastia, F. Lacroute, A family of low and high copy replicative, integrative and single-stranded *S. cerevisiae*/*E. coli* shuttle vectors. *Yeast* **7**, 609–615 (1991).

Acknowledgments: We thank A. Rodríguez-Navarro (Universidad Politécnica de Madrid, Spain) for providing the plasmid pFL61 *At*AKT1 and G. Garijo [Universidad Pública de Navarra (UPNa)] and J. Melo [Faculdade de Ciências da Universidade de Lisboa (FCUL)] for technical assistance. Stable isotope ratio analyses were performed at the Stable Isotopes and Instrumental Analysis Facility of the Centre for Ecology, Evolution and Environmental Changes (cE3c), University of Lisbon–Portugal. **Funding:** I.A. was supported by a postdoctoral fellowship from the Government of Navarra, Spain (Anabasid outgoing Programme, 2011) and by a postdoctoral fellowship from the Portuguese Fundação para a Ciência e a Tecnologia (SFRH/BPD/90436/2012). A.M.M. is a senior research associate of the Belgian Fonds de la Recherche Scientifique Fonds de la Recherche Scientifique–FNRS (grants CDR J017617F, PDR T011515F, and ARC) and a WELBIO investigator, and M.B. is a scientific research worker supported by WELBIO. This work was also developed in the context of the following projects: PTDC/BIA-BEC/099323/2008 and PTDC/AGR-PRO/115888/2009 to cE3c and FCUL, UID/DTP/04138/2013 to iMed.ULisboa, and AGL2015-64582-C3-1-R and AGL2012-37815-C05-05 to UPNa. **Author contributions:** I.A., C.C., and P.M.A.-T. conceived and designed all the experiments. A.M.M., M.B., and N.v.W. contributed to design growth conditions and pH experiments. I.A. and C.G. performed experiments. M.B. performed yeast transformations (except to CrAMTs) and helped to analyze results of pH experiments. E.S.-L. performed yeast transformations with CrAMTs. A.P.M., G.S., I.A., and P.M.A.-T. performed stopped-flow experiments. A.P.M. and G.S. analyzed data and contributed to writing the part of stopped-flow experiments. I.A. analyzed the data of the rest of the experiments. I.A., C.C., P.M.A.-T., A.M.M., and N.v.W. wrote the paper with helpful contribution from M.B., E.F., and E.S.-L. I.A. performed statistical analysis. **Competing interests:** The authors declare that they have no competing interests. **Data and materials availability:** All data needed to evaluate the conclusions in the paper are present in the paper and/or the Supplementary Materials. Additional data related to this paper may be requested from the authors.

Submitted 3 November 2017
Accepted 27 July 2018
Published 12 September 2018
10.1126/sciadv.aar3599

Citation: I. Ariz, M. Boeckstaens, C. Gouveia, A. P. Martins, E. Sanz-Luque, E. Fernández, G. Soveral, N. von Wirén, A. M. Marini, P. M. Aparicio-Tejo, C. Cruz, Nitrogen isotope signature evidences ammonium deprotonation as a common transport mechanism for the AMT-Mep-Rh protein superfamily. *Sci. Adv.* **4**, eaar3599 (2018).